In Vivo Chemical and Structural Analysis of Plant Cuticular Waxes Using Stimulated Raman Scattering Microscopy[1][OPEN]

George R. Littlejohn[2], Jessica C. Mansfield[2], David Parker, Rob Lind, Sarah Perfect, Mark Seymour, Nicholas Smirnoff, John Love*, and Julian Moger*

School of Biosciences, College of Life and Environmental Sciences (G.R.L., N.S., J.L.), and Department of Physics and Astronomy, College of Engineering, Mathematics, and Physical Sciences (J.C.M., J.M.), University of Exeter, Exeter, Devon EX4 4QD, United Kingdom; Biodomain Technology Group, Shell International Exploration and Production, Inc., Westhollow Technology Center, Houston, Texas 77082 (D.P.); and Syngenta, Jealott's Hill International Research Centre, Bracknell, Berkshire RG42 6EY, United Kingdom (R.L., S.P., M.S.)

ORCID IDs: 0000-0002-8768-2598 (G.R.L.); 0000-0003-2191-6416 (D.P.); 0000-0002-1410-4033 (R.L.).

The cuticle is a ubiquitous, predominantly waxy layer on the aerial parts of higher plants that fulfils a number of essential physiological roles, including regulating evapotranspiration, light reflection, and heat tolerance, control of development, and providing an essential barrier between the organism and environmental agents such as chemicals or some pathogens. The structure and composition of the cuticle are closely associated but are typically investigated separately using a combination of structural imaging and biochemical analysis of extracted waxes. Recently, techniques that combine stain-free imaging and biochemical analysis, including Fourier transform infrared spectroscopy microscopy and coherent anti-Stokes Raman spectroscopy microscopy, have been used to investigate the cuticle, but the detection sensitivity is severely limited by the background signals from plant pigments. We present a new method for label-free, in vivo structural and biochemical analysis of plant cuticles based on stimulated Raman scattering (SRS) microscopy. As a proof of principle, we used SRS microscopy to analyze the cuticles from a variety of plants at different times in development. We demonstrate that the SRS virtually eliminates the background interference compared with coherent anti-Stokes Raman spectroscopy imaging and results in label-free, chemically specific confocal images of cuticle architecture with simultaneous characterization of cuticle composition. This innovative use of the SRS spectroscopy may find applications in agrochemical research and development or in studies of wax deposition during leaf development and, as such, represents an important step in the study of higher plant cuticles.

The majority of land plants possess an extracellular, waxy cuticle that covers the surface of their aerial parts and protects them against desiccation, external physical and chemical stresses, and a variety of biological agents (Grncarevic and Radler, 1967; Barthlott and Neinhuis, 1997; Krauss et al., 1997; Ristic and Jenks, 2002; Yeats and Rose, 2013). The cuticle is a composite layer composed mainly of cutin and overlaid by cuticular waxes. Cutin is a macromolecular structure consisting primarily of hexadecanoic (palmitic) and octadecenoic (vaccenic) acids that are covalently linked by ester bonds to generate a rigid, three-dimensional network that is embedded with polysaccharides. Cuticular waxes are composed of long-chain (C_{20}–C_{40}) aliphatic molecules derived from fatty acids (Samuels et al., 2008), and studies over the last several decades have identified structural and regulatory constituents of the biosynthetic pathways of cuticular components (Kolattukudy, 1981; Beisson et al., 2012). In addition to the physiochemical properties conferred by its lipid components, the architecture of the cuticle plays an essential role in physiological function. For example, through understanding the properties of the cuticular structure, the extraordinary superhydrophobicity of the *Lotus* spp. leaf has been mimicked in micro- and nanotechnology to generate self-cleaning surfaces (Bhushan and Jung, 2006; Bhushan et al., 2009; Koch et al., 2009).

As may be expected, given the diversity of plants, the habitats they inhabit, and individual life histories, the morphology and composition of plant cuticle varies extensively between and within species and includes plate-, needle-, and pillar-shaped wax crystals (Barthlott et al., 2008). In some species, cuticular wax composition is known to vary with depth, giving rise to chemically distinguishable layers (Yeats and Rose, 2013). Finally, the cuticle is increasingly shown to be important in development (Koornneef et al., 1989; Yeats and Rose,

[1] This work was supported by the Biotechnology and Biological Sciences Research Council (grant to J.L. and J.M.), Shell Research Ltd. (grant to J.L.), and Syngenta (grant to J.M.).

[2] These authors contributed equally to the article.

* Address correspondence to j.moger@exeter.ac.uk and j.love@exeter.ac.uk.

The author responsible for distribution of materials integral to the findings presented in this article in accordance with the policy described in the Instructions for Authors (www.plantphysiol.org) is: Julian Moger (j.moger@exeter.ac.uk).

J.M. conceived the project; J.M., J.L., and N.S. designed the experiments; G.R.L. and J.C.M. performed the experiments; G.R.L., J.C.M., D.P., R.L., S.P., M.S., N.S., J.L., and J.M. analyzed the data; D.P., R.L., S.P., and M.S. contributed reagents and performed the analyses; G.R.L., J.C.M., N.S., J.L., and J.M. wrote the article.

[OPEN] Articles can be viewed without a subscription.

www.plantphysiol.org/cgi/doi/10.1104/pp.15.00119

2013) and pathogenesis (Lee and Dean, 1994; Gilbert et al., 1996; Bessire et al., 2007; Delventhal et al., 2014). It is therefore unsurprising that interest in cuticle composition, structure, and physiology is increasing (Buschhaus et al., 2014; Hen-Avivi et al., 2014; Heredia-Guerrero et al., 2014; Xu et al., 2014). Moreover, a greater understanding of the relationship between structure and chemical composition of cuticle waxes is vital for enhancing agriculture yields, as it will further our knowledge of how plants regulate water balance and inform the application of nutrition (foliar feeds) and pesticides, leading to improved formulation strategies for agrochemicals.

The chemical composition and topological architecture of cuticular waxes are both critical for optimal physiological function. Analyses of these essential properties have typically been performed separately. Cuticle wax composition is normally determined using gas chromatography; cuticle ultrastructure may be analyzed using destructive imaging techniques such as scanning electron microscopy (SEM; Baker and Holloway, 1971; Jetter et al., 2000; Barthlott et al., 2008) and laser desorption ionizing mass spectroscopy (Jun et al., 2010) or, in vivo, using nondestructive real-time techniques, including white-light scanning interferometry (Kim et al., 2011), atomic force microscopy (Koch et al., 2004), confocal microscopy in reflectance mode (Veraverbeke et al., 2001), fluorescence microscopy of chemical stains (Pighin et al., 2004), coherent anti-Stokes Raman scattering (CARS) microscopy (Yu et al., 2008; Weissflog et al., 2010), and total internal reflection Raman spectroscopy (Greene and Bain, 2005). Despite the advances in our understanding of the cuticle that have been made with these techniques, there is a great need for techniques that combine chemical and structural information to provide in situ high-resolution chemical analysis of epicuticle waxes.

Techniques based on vibrational spectroscopy offer in situ chemical analysis derived from the vibrational frequencies of molecular bonds within a sample. However, due to water absorption and the intrinsically low spatial resolution associated with the long infrared (IR) wavelengths required to directly excite molecular vibrations, IR absorption techniques have limited value for bioimaging. Raman scattering, however, provides analysis of vibrational frequencies by examining the inelastic scattering of visible light. Raman scattered light is frequency shifted with respect to the incident light by discrete amounts that correspond to the vibrational frequencies of molecular bonds within the sample. The spectrum of Raman scattered light consists of a series of discrete peaks that each correspond to a molecular bond and can be regarded as a chemical fingerprint holding a wealth of information regarding chemical composition. Unfortunately, Raman scattering is an extremely weak effect, and typical signals from biological samples are at least six orders of magnitude weaker than those from fluorescent labels. This severely limits the application of Raman for studying living systems because long acquisition times (100 ms–1 s per pixel) and relatively high excitation powers (several hundred milliwatts) are required to image most biomolecules with sufficient sensitivity. Furthermore, the lack of sensitivity is compounded by autofluorescence, which in plant tissues completely overwhelms the Raman signal, prohibiting its application in planta.

Far stronger Raman signals can be obtained using coherent Raman scattering (CRS; Min et al., 2011). CRS achieves a Raman signal enhancement by focusing the excitation energy onto a specific molecular vibrational frequency (Fig. 1A). A pump and Stokes beam, with frequencies ω_p and ω_S, respectively, are incident upon the sample, with their frequency difference (ω_p–ω_S) tuned to match the molecular vibrational frequency of interest. Under this resonant condition, the excitation fields efficiently drive bonds to produce a strong nonlinear coherent Raman signal. When applied in microscopy format, the nonlinear nature of the CRS process confines the signal to a submicron focus that can be scanned in space, allowing three-dimensional confocal-like mapping

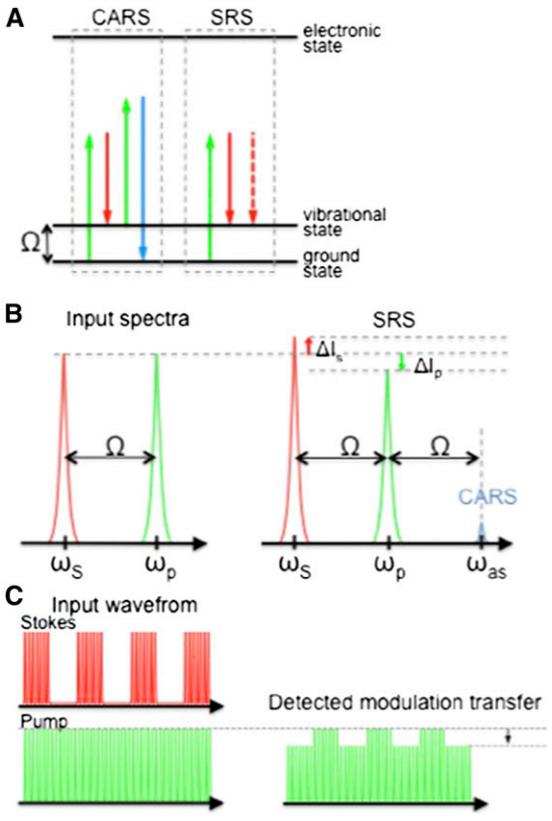

Figure 1. Schematic representation of the two CRS processes: CARS and SRS. A, Energy level diagrams for the CARS and SRS processes, showing the pump (green), Stokes (red), and anti-Stokes (blue) photon energies. B, Diagrammatic representation of the input and output spectra for CARS and SRS, showing the gain and loss in the pump (red) and Stokes (green) beams, respectively. ΔI_S, Change in Stokes beam intensity; ΔI_p, change in pump beam intensity. C, Diagrammatic representation of the modulation transfer detection scheme used to detect stimulated Raman gain and loss with high sensitivity.

of biomolecules. CRS microscopy has particular advantages for bioimaging: (1) Chemically specific contrast is derived from the vibrational signature of endogenous biomolecules within the sample, negating the need for extraneous labels/stains; (2) Low-energy, near-IR excitation wavelengths can be employed, which reduces photodamage and increases depth penetration into scattering tissues; and (3) The CRS process does not leave sample molecules in an excited state, does not suffer from photobleaching, and can be used for time course studies.

CRS microscopy may be achieved by detecting either CARS or stimulated Raman scattering (SRS).

CARS MICROSCOPY

CARS microscopy relies on detection of the anti-Stokes signal generated at frequency $\omega_{as} = 2\omega_p - \omega_S$, which, by using filters, is spectrally isolated from the pump and Stokes beams, and its intensity is used to map the location of biomolecules of interest (Zumbusch et al., 1999). The CARS signal is blue shifted with respect to the pump and Stokes wavelengths (Fig. 1B), making CARS more resilient to sample autofluorescence than spontaneous Raman. However, in highly autofluorescent samples such as plant tissues, the usually weak two-photon fluorescence (also blue shifted with respect to the excitation wavelengths) overwhelms the CARS signal. Consequently, CARS imaging in planta has only been applied to samples with reduced chlorophyll autofluorescence including dried tissues (Zeng et al., 2010; Ding et al., 2012), roots (Ly et al., 2007), and cuticle waxes after they have been stripped away from the leaf (Weissflog et al., 2010).

SRS MICROSCOPY

SRS relies on detecting subtle changes in the intensities of the excitation fields that occur by virtue of stimulated excitation (Freudiger et al., 2008). When the difference frequency, $\omega_p - \omega_S$, matches the frequency of a molecular vibration, the Stokes beam intensity experiences a gain, while the intensity of the pump beam experiences a loss, shown in Figure 1C. This transfer of intensity between the excitation beams only occurs when both beams are incident simultaneously on the sample and is measured by detecting the modulation that is transferred to the pump beam after it has passed through the sample when the intensity of the Stokes beam is modulated. The amplitude of the transferred intensity modulation is directly proportional to the concentration of target molecules and, by modulating at frequencies above laser noise (>1 MHz), can be detected with a lock-in amplifier with great sensitivity (Ye et al., 2009).

Because SRS is detected at the same wavelength as the excitation fields, it is not affected by fluorescent emission and, as recently demonstrated by Mansfield et al. (2013), may also be used in the presence of highly pigmented samples such as plant tissues.

We have recently shown that it is possible use phase-sensitive detection to separate the vibrational SRS signal from the electronic absorption processes (Mansfield et al., 2013). In this investigation, we used SRS imaging to investigate both the structure and chemical composition of plant cuticular waxes, simultaneously and in vivo. We compared SRS images of cuticle wax structures from a variety of plant species that display characteristic wax morphologies with SEM and CARS images of the leaf surface. We demonstrated that spectroscopic information can be obtained to provide chemically specific, in situ analysis of waxes on living leaves with submicron spatial resolution. Using SRS microscopy, we compared the cuticle structure and composition between wild-type Arabidopsis (*Arabidopsis thaliana*) and an *eciferum1* (*cer1*) mutant with impaired cuticle deposition and have also shown that SRS imaging is sufficiently sensitive to track temperature-induced changes in cuticle formation in *Thellungiella salsuginea*. We conclude that, with the increasing availability of commercial Raman-based microscopes, SRS imaging has the potential to radically advance our understanding of plant cuticular structure and composition and their effects on physiology and development.

RESULTS

Characterization of the Raman Spectra of Dissolved Cuticle Waxes

Spontaneous Raman spectra of hexane-extracted wax samples over the CH vibrational region from 2,700 to 3,200 cm^{-1} were acquired as a baseline reference for each plant species (Fig. 2). Gaussian peaks were fitted underneath each of the spectra to visualize the relative contribution of different molecular vibrations, based on peaks previously identified in the literature (Snyder et al., 1978; Ho and Pemberton, 1998; Greene and Bain, 2005). The wax extracts from Arabidopsis, *Thellungiella parvula*, banana (*Musa acuminata*), and cheese plant (*Monstera delicosa*) had similar spectral profiles that matched those reported for other waxes and alkanes reported in the literature (Snyder et al., 1978; Greene and Bain, 2005) and deconvolved into seven identifiable peaks (Table I). The peaks, corresponding to the symmetrical and antisymmetrical CH_2 stretch, are prominent on all spectra. The ratio antisymmetric-to-symmetric peak height is known to give a strong indication of the alkyl chain conformational order with a ratio of 1.6 to 2 indicating a highly crystalline structure, and a ratio of 0.6 to 0.9 indicating a liquid structure (Snyder et al., 1978; Ho and Pemberton, 1998, Greene and Bain, 2005). For the wax samples analyzed here, the ratios were as follows: Arabidopsis, 1.13; *T. parvula* 1.58; banana, 1.34; and cheese plant, 1.54; indicating structures intermediate between a highly crystalline structure and a liquid. The curve fits to the spectra also included two Fermi resonances of the CH_2 bond one at 2,930 cm^{-1} and another very broad Fermi resonance at approximately 2,870 cm^{-1} (Snyder et al., 1978). The contributions due to

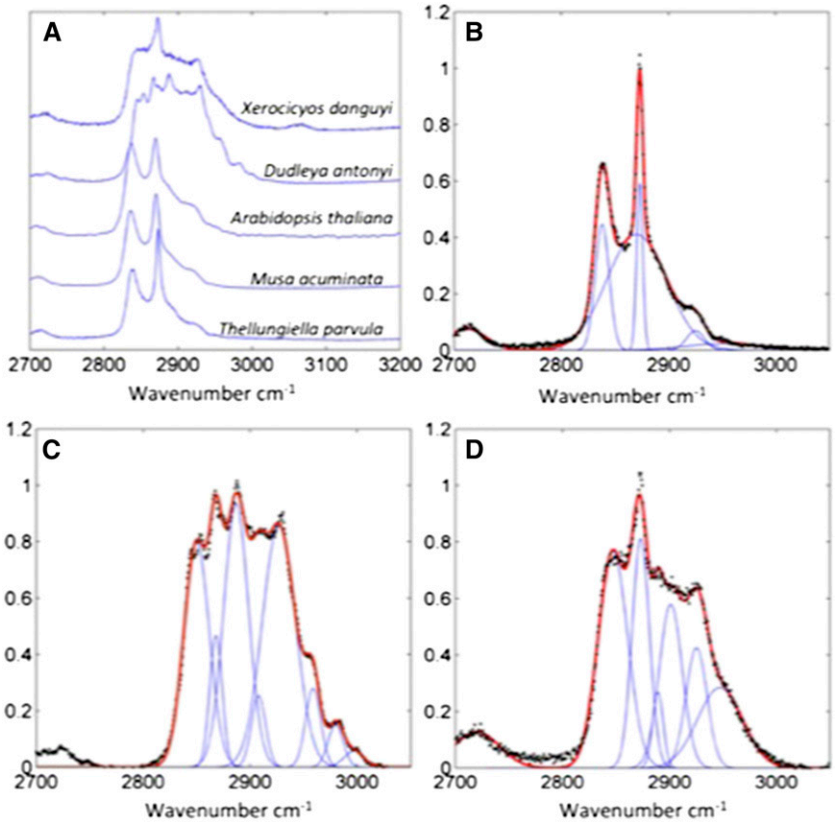

Figure 2. Raman spectra and curve fits of plant leaf waxes. A, Raman spectra of cuticle waxes purified from silver dollar plant, *D. anthonyi*, Arabidopsis, banana, and *T. parvula*. Peak fitting to the Raman spectra of *T. parvula* (B), *D. anthonyi* (C), and silver dollar plant (D).

the CH_3 symmetric and antisymmetric stretches were small, as proportionally there are much less of these groups due to the long chain lengths. The fitting parameters for each wax along with the goodness of fit are included in Supplemental Text S1.

Two of the species investigated, *Dudleya anthonyi* and silver dollar plant (*Xerosicyos danguyi*), showed dramatically different Raman spectra from Arabidopsis, *T. parvula*, banana, and cheese plant, characterized by additional peaks, which are indicative of a more complex chemical structure, with additional chemical bonds to those described in Table I. In *D. anthonyi*, the Raman spectrum changed depending on the number of the hexane wash and hence, we surmise, on the depth of penetration into the cuticle; the initial, most superficial hexane wash showed an unusual Raman spectrum, but subsequent washes that solubilize waxes deeper in the cuticle showed spectra that matched more closely with those of a typical alkane. These differences are most readily explained by both these species possessing a thick, glaucous cuticle compared with the other plant species studied, an adaptation enabling survival in xeric environments.

In Vivo Comparison of CARS and SRS Images of Plant Cuticle

Having characterized the Raman spectra of waxes extracted from the cuticle of a variety of plants, we imaged the cuticles of the same plants in vivo, using both CARS microscopy (Weissflog et al., 2010) and SRS microscopy (Fig. 3). SRS and CARS images of the epicuticular wax layer of *T. parvula* leaves were acquired simultaneously (Fig. 3) and are presented as the exemplar to compare the two techniques.

The images acquired using CARS are dominated by high levels of background autofluorescence from cell walls and chloroplasts (Fig. 3A). This autofluorescence is due to inevitable two-photon absorption by the compounds in these organelles and the resulting fluorescence emission at similar wavelengths to the CARS signal. Consequently, in the CARS images, only the largest wax crystals can be visualized.

Conversely, in the SRS image (Fig. 3B), there is no fluorescent background because the signal measured is

Table I. *Raman peaks used in curve fitting for cuticular waxes*

Peak Wavelength (Approximate)	Assignment
2,840 (crystalline) 2,850 (liquid)	CH_2 symmetric stretch
2,870 (crystalline) 2,880 (liquid)	CH_2 antisymmetric stretch
2,930	CH_2 Fermi resonance
2,952	CH_2 antisymmetric (out of plane)
2,964	CH_2 antisymmetric (in plane)
2,880 to 2,901	CH_2 symmetric
2,870 (very broad)	CH_2 Fermi resonance

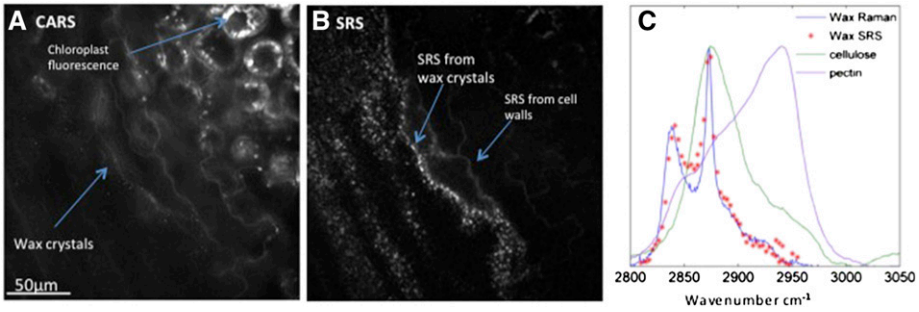

Figure 3. CARS and SRS images of the *T. parvula*leaf surface. The surface of a leaf from *T. parvula* was simultaneously imaged using CARS microscopy (A) and SRS microscopy (B). Both images were acquired at a 2,845 cm^{-1} CH_2 symmetric stretch. The CARS image (A) is dominated by autofluorescence, and only the largest wax crystals are visible against the background. Conversely, the SRS image (B) is almost background free, enabling the cell walls and wax crystals to be clearly visualized. C shows the spectral scan of the SRS (red crosses) from the wax crystals in situ overlaid onto the spontaneous Raman spectra of purified *T. parvula* wax (blue line), purified cellulose (green line), and purified pectin (purple line).

not due to a change in wavelength (i.e. fluorescence relative to excitation) but a change in intensity between the excitation lasers (the pump and Stokes beams) following stimulated Raman excitation of the samples. The cuticular wax crystals are clearly visible, and the SRS signal spectrally matches that of the spontaneous Raman spectrum of purified cuticular waxes (Fig. 3C). Cell walls are also visible in the SRS images, although with a lesser intensity than the wax crystals, which can be explained by the overlap between the Raman spectra

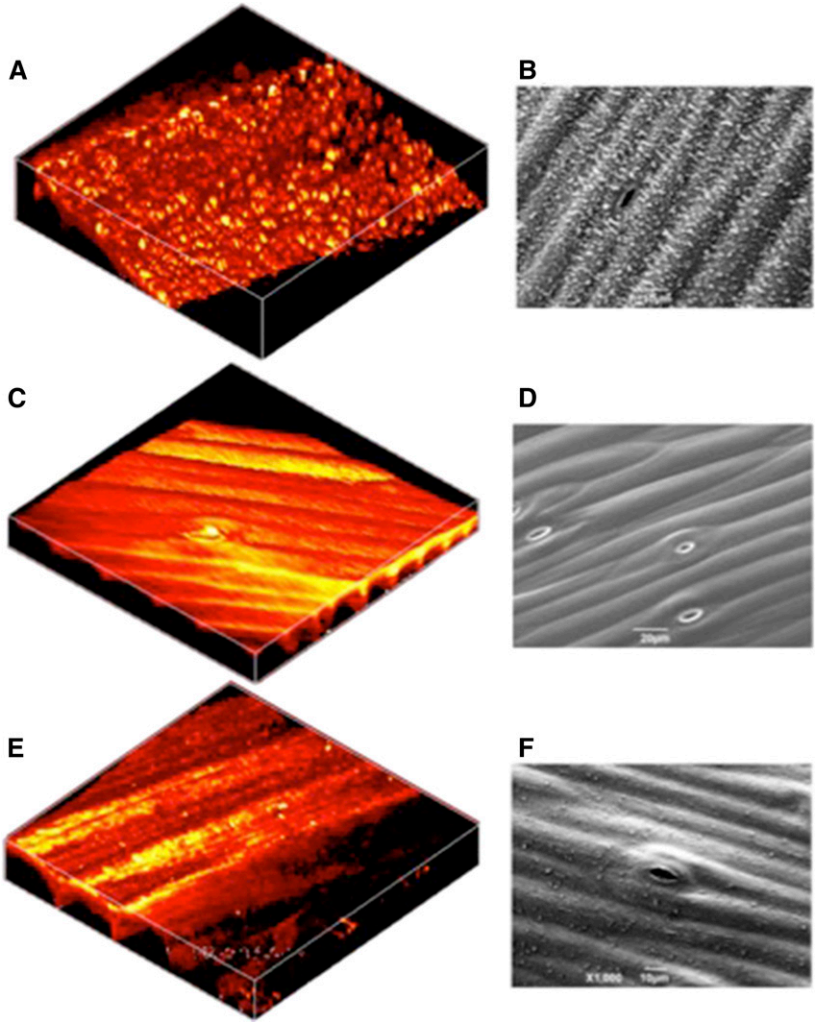

Figure 4. SRS images and scanning electron micrographs of Arabidopsis cuticle. The surface of Arabidopsis stems were imaged using SRS microscopy (A, C, and D) and SEM (B, D, and E). A and B, The surface of the untreated stem of wild-type Arabidopsis, ecotype Landsberg *erecta*, with the structure of cuticle wax crystals clearly visible. C and D, The surface of the wild-type Arabidopsis stem following a wash in hexane that dissolved the cuticle waxes. E and F, The surface of the stem from a *cer1* Arabidopsis mutant. A, C, and E were generated from three-dimensional stacks taken of a 64- × 64-μm field of view and are displayed in false color.

of the cuticular waxes and cellulose. SRS microscopy therefore, not only provides clearer images of plant cuticle structure than CARS microscopy, but, because of the low levels of background noise in the images, also has the capacity to yield information on specific compounds that compose the imaged structures.

Comparison of SRS and Scanning Electron Microscope Images of Plant Cuticle

To confirm the capacity of SRS microscopy for accurately resolving cuticular structures, the surface of Arabidopsis stems were imaged using SRS microscopy and the more conventional SEM (Fig. 4). SRS and SEM images of untreated, wild-type stems (Fig. 4, A and B) show an uneven surface composed of similarly proportioned globules, although the level of detail is higher in the SEM image. We ascertained that these globular structures were waxes by washing the stems in hexane prior to imaging (Fig. 4, B and C). In this case, both images show that the surface of the stem is smooth, with clearly visible cells and stomata. Finally, stems from Arabidopsis defective for *CER1* gene expression were imaged using either technique (Fig. 4, E and F). *cer1* mutants are impaired in cuticle wax biosynthesis (Aarts et al., 1995; Bernard et al., 2012), and the images show stems with markedly reduced surface structures compared with the wild type (Fig. 4, A and B).

Unlike SEM, which provides information only on the surface topology of imaged samples, SRS microscopy is a technique of multiphoton confocal microscopy that, like conventional confocal microscopy, can penetrate materials and provide information on their subsurface structure. To illustrate this technical capability, we imaged the cuticles of banana and silver dollar plant (Fig. 5). Banana was chosen, as it is a monocot, with a visibly waxy cuticle and regular files of elongated, epidermal cells. Silver dollar plant was chosen because of its thick, glaucous cuticle composed of different waxes with different Raman spectra.

Three-dimensional reconstructions of confocal SRS images of banana (Fig. 5, A and C) and silver dollar plant (Fig. 5, B and C) cuticles show very different structures. The banana cuticle is formed of a number of hair-like projections from the leaf surface. In the comparator SEM image (Fig. 5E), these projections clump together, most likely due to the process of fixation, and show a less even distribution. By contrast, the silver dollar plant cuticle has an amorphous surface, supported by a

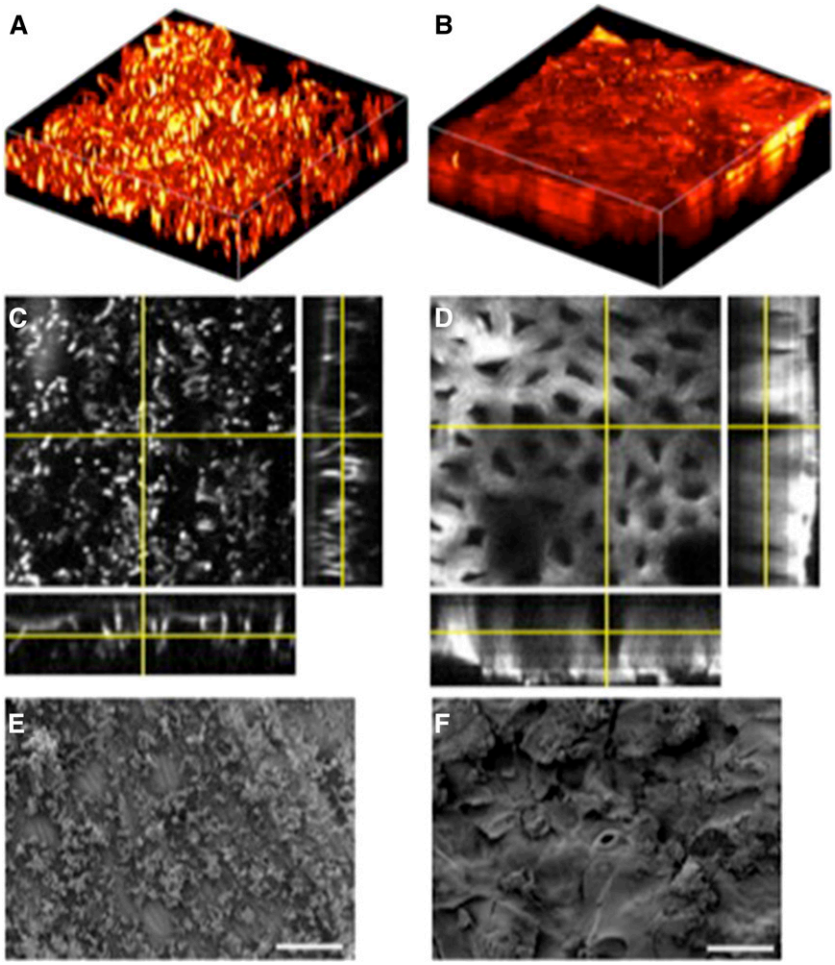

Figure 5. SRS images and scanning electron micrographs of cuticle of banana and of silver dollar plant. The surface of banana and of silver dollar plant leaves were imaged using SRS microscopy (A–D) and SEM (E and F). A, An SRS image of the adaxial leaf surface of surface banana constructed from an image stack from a 64- × 64-μm field of view. B, An SRS image of silver dollar plant leaf reconstructed from an image stack from a 126- × 126-μm field of view. C and D, Orthogonal views projected from the image stacks presented in A and B, respectively, showing the depth profile of cuticles. E and F, SEM images of the cuticles of banana and silver dollar plant leaves, respectively.

reticulate pattern (6–10 μm below the surface) of columnar structures emerging from the leaf epidermis. The amorphous surface of the silver dollar plant cuticle is clear on the comparator SEM image (Fig. 5F), but the intriguing cuticle substructure is not.

The comparison between SRS and SEM images therefore demonstrates that sufficient contrast can be produced using SRS microscopy to provide credible, structural images of waxes with submicron resolution that correlate well with images from SEM and can provide critical, structural information not previously available.

Simultaneous Ultrastructural Imaging and Chemical Analysis of Cuticle by SRS Microscopy

As previously noted, SRS imaging relies on the chemically specific Raman spectrum of the cuticle constituents. To verify the potential of the technique to provide structural and chemical information, simultaneously and in vivo, we first analyzed the cuticle of *D. anthonyi* (Fig. 6). *D. anthonyi*was selected for this aspect of the investigation because previous work had shown stratification of the composition of cuticular wax in the *D. anthonyi* cuticle (Jetter et al., 2000).

Both the SRS (Fig. 6A) and SEM (Fig. 6B) images of the *D. anthonyi* cuticle show a complex structure; the outer cuticle layer has a structure in which many small wax crystals are amassed together, with the deeper layers of the cuticle having a smoother, somewhat reticulated or wavelet-like appearance (Fig. 6D). Most importantly for this investigation, it is clear that the wax composition, as reported by the SRS spectra (Fig. 6C), was different depending on cuticle depth. The SRS spectrum acquired from deeper in the cuticle was most similar to an alkane, whereas the SRS spectrum from the surface components was markedly different, indicating a different chemical composition.

It is well documented that changes in wax composition and deposition during development and in response to abiotic stress or pathogen attack are important in the life history of many plant species (Raffaele et al., 2009; Bourdenx et al., 2011). *T. salsuginea* is particularly interesting because it is a close relative of Arabidopsis and *T. parvula*, and its cuticle composition and structure alters following exposure to prolonged cold treatment or vernalization (Teusink et al., 2002; Amtmann, 2009; Xu et al., 2014).

To determine whether SRS microscopy could, in principle, document the ultrastructural and chemical changes in cuticle that may occur during plant development, we imaged leaves from *T. salsuginea* plants that had been grown either in constant temperature or exposed to a 14-d-long cold shock using SRS microscopy and SEM (Fig. 7). Plants grown at a constant temperature of 20°C show a cuticle containing aggregates of waxes on the adaxial surface of the leaf (Fig. 7, A and B) and relatively little cuticular waxes on the abaxial surface (Fig. 7, C and D). However, following incubation at 4°C for 14 d, a marked alteration in cuticle structure can be observed on both the adaxial and abaxial surfaces (Fig. 7, C–H): a marked increase in waxy deposits in the cuticle was observed covering the entire leaf. Moreover, the ultrastructural aggregation of the cuticle waxes was smaller and more regular than that observed on the adaxial surface of leaves grown in a constant temperature of

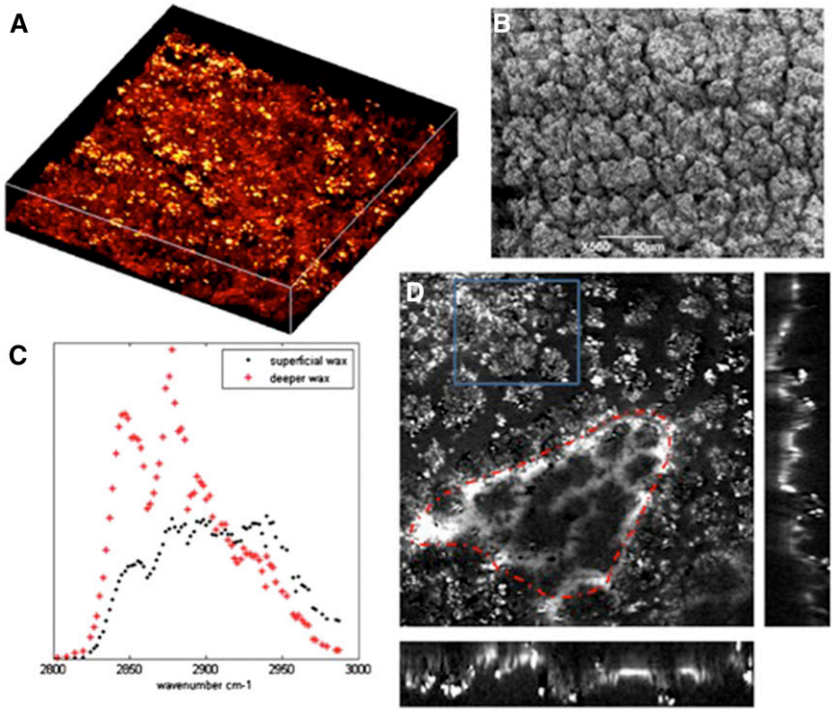

Figure 6. SRS spectral images of *D. anthonyi* cuticle. SRS spectral imaging of *D. anthonyi* cuticle waxes shows changes in chemical composition with depth. A and B, The SRS and SEM images, respectively, of *D. anthonyi* leaf showing the crystalline structure of cuticle wax deposits on the adaxial surface. The image in A is a three-dimensional reconstruction of an image stack taken from a 126- × 126-μm field of view at the 2,840 cm^{-1} Raman shift. C, SRS spectral scans taken from the more superficial and deeper wax areas indicated on D. Blue rectangle, An area of superficial wax; red line, an area deeper in the cuticle. The imagess on the right and bottom of the main image in D are from the orthogonal views through the stack showing the depth profile image of the cuticle wax.

20°C (Fig. 7, A and B). SRS microscopy therefore precisely reported the anticipated changes in cuticle formation that occur following exposure to cold in *T. salsuginea* and, by extension, may prove a useful, in vivo tool for investigating other dynamic changes in cuticle architecture and composition during development and in response to environmental or biotic perturbation.

DISCUSSION

The cuticle is a composite, hydrophobic layer composed mainly of waxes and cutin secreted from the aerial epidermis of land plants. The cuticle performs a number of physiological roles, notably acting as a barrier to water loss, which, in higher plants, enables the exquisite control of evapotranspiration by stomatal guard cells, increasing light reflection and heat tolerance in xerophytes and providing an essential barrier to the ingress of toxins and pathogens into the plant. Cuticle topography and composition has mainly been investigated using destructive techniques that provide only a fragmented understanding of the complexity of this essential structure.

In this investigation, we have generated in vivo images of cuticle waxes at submicron resolution, using SRS microscopy. Like other forms of nonlinear Raman-based imaging techniques, SRS is label free and enables the simultaneous acquisition of chemically specific data and confocal quality images. Most importantly, SRS microscopy relies on a change in signal intensity rather

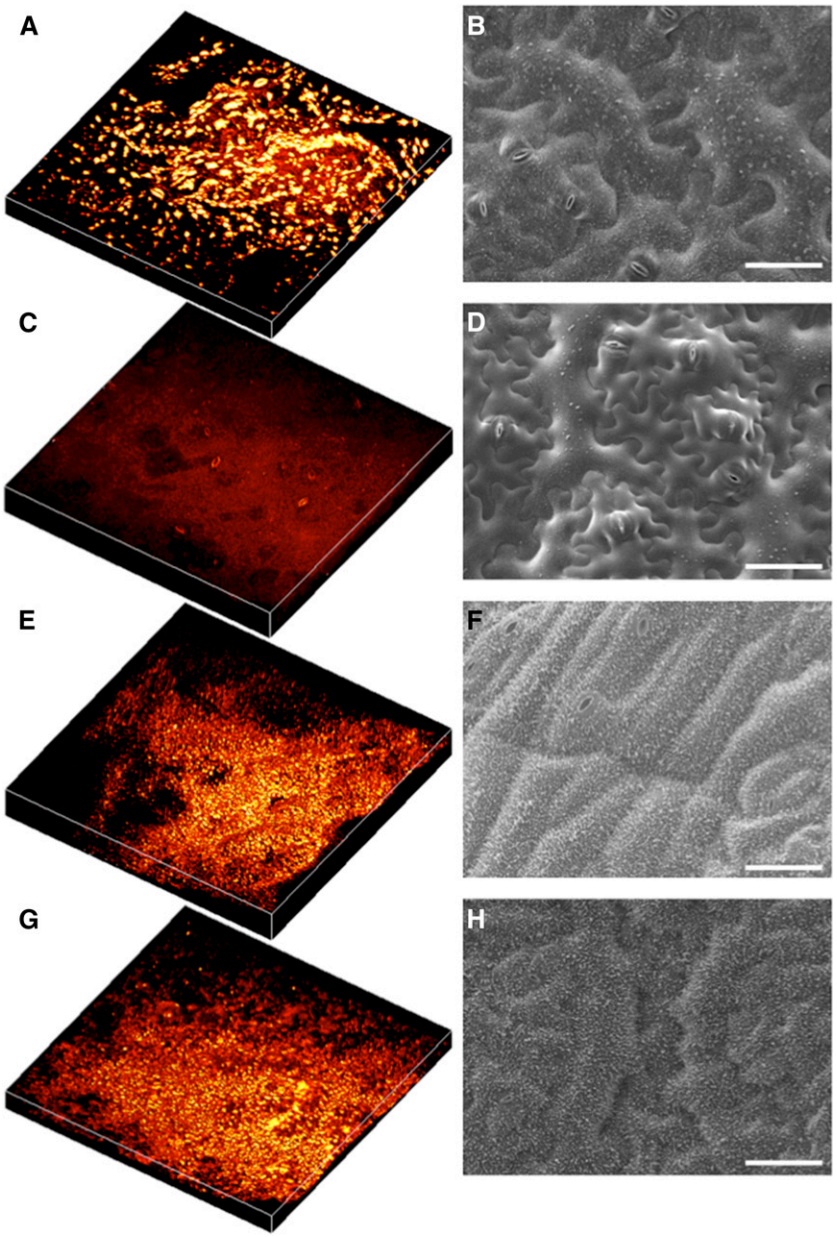

Figure 7. SRS images and scanning electron micrographs of the cuticle of *T. salsuginea* following cold-induced wax biogenesis. *T. salsuginea* leaves were imaged using SRS spectral imaging and SEM before and after cold treatment. A, C, E, and G, Three-dimensional reconstructions of image stacks from a 250- × 250-μm field of view at the 2,840 cm^{-1} Raman shift. B, D, F, and H, SEM images. A to D are, respectively, from the adaxial and abaxial leaf surfaces of plants grown at 20°C for 8 weeks. E to H are, respectively, from adaxial and abaxial leaf surfaces of plants grown at 20°C for 4 weeks and then at 4°C for 2 weeks and at 20°C for an additional 2 weeks. Bars = 50 μm.

than wavelength, so images can be acquired without the strong autofluorescent background from chloroplasts and cell walls that hampers the resolution and interpretation of CARS and spontaneous Raman images (Gierlinger et al., 2010, 2012).

The structures observed using SRS microscopy compared well to those seen under the SEM, albeit with a lesser degree of resolution due to the inherent limitations of optical microscopy relative to electron microscopy. However, unlike SEM, which generates images from the surface of fixed or cryogenically preserved samples, SRS imaging, like other forms of single- or multiphoton laser microscopy, enables information to be acquired in vivo from within the sample and three-dimensional reconstructions of internal structures to be reconstructed. This capacity is particularly advantageous for documenting dynamic changes of topography or composition that may occur and that are otherwise undetectable using fixed samples.

As demonstrated here, the chemical specificity of the SRS signal allows differentiation of different wax components from the main constituents of cell walls, cellulose, and pectins. In this study, we showed that the xerophytes *D. anthonyi* and silver dollar plant had different cuticular wax compositions from the other mesophytic plants investigated. Although this result is unsurprising, as these plants were selected for precisely their singularly thick and glaucous cuticles, it does demonstrate the potential of SRS for in vivo characterization of cuticle constituents. Moreover, although we did not attempt in this study to quantify, in situ, the different compounds for which we acquired SRS spectra, it may be possible to use this technique in a more quantifiable manner to characterize, in vivo, the relative abundance of cuticle or cell wall components and the changes that may occur in response to environmental or developmental stimuli. In this investigation, we have shown that SRS imaging is sufficiently sensitive enough to show developmental changes in wax production in *T. salsuginea*. Moreover, the technique may be useful for characterizing wax biosynthesis mutants, such as the exemplar used here, cer1, which has been shown to have a role in both water use and Arabidopsis interaction with fungal and bacterial pathogens (Raffaele et al., 2009; Bourdenx et al., 2011). SRS microscopy may therefore provide new insights into the physiological responses of plants to drought, temperature, chemicals, or pathogens and underpin the use of alternative model systems, such as *T. salsuginea* (Amtmann 2009), to investigate the control of cuticle deposition.

However promising, any new technology or application must be simplified to enable widespread use. Currently, SRS microscopy is somewhat niche and requires specialist knowledge. However, commercial, user-friendly CARS microscopes that can be converted to SRS imaging exist and, like laser confocal microscopy, will become increasingly common and add real-time, label-free Raman microscopy to the range of imaging techniques widely available to researchers in plant science.

CONCLUSION

The chemical composition and structure of the cuticle in mesophyllous plants are crucial elements for survival, physiology, and development. We have shown that SRS microscopy can be used to acquire in vivo, three-dimensional images of the cuticle in a variety of plant species, enabling simultaneous analysis of cuticle structure and chemical composition. In contrast to CARS microscopy, which is more common, SRS images of plant tissues contain very low autofluorescence from chloroplasts or cell walls and are therefore easier to interpret. Moreover, SRS images compare well with those acquired using SEM, albeit with the lower resolution that is due to the use of laser light rather than an electron beam. Moreover, we have shown that SRS can be used to track and quantify dynamic changes in cuticle structure and composition in response to environmental stimuli and can therefore increase our understanding of this essential and often-overlooked structure.

MATERIALS AND METHODS

Plants

Silver dollar plant (*Xerosicyos danguyi*), *Dudleya anthonyi*, banana (*Musa acuminate*), and cheese plant (*Monstera delicosa*) were grown in soil in the University of Exeter greenhouses and harvested between February and April 2012. The photoperiod was set to 16 h, from 5 AM to 9 PM. Supplemental lighting and shading were provided to ensure irradiance between 540 and 720 μmol s^{-1} m^{-2}. The greenhouse temperature was set to 19.5°C with an SD of 3.7°C. Arabidopsis (*Arabidopsis thaliana*), *Thellungiella salsuginea*, and *Thellungiella parvula* were grown in a 16-h-light/8-h-dark photoperiod at 20°C in growth rooms controlled for temperature and humidity. Four weeks after germination, the *Thellungiella* spp. were transferred to an ambient temperature of 4°C for 2 weeks and then returned to 20°C for an additional 2 weeks. The light regime remained at 16 h of light/8 h of dark during all experiments. Leaves were harvested for imaging and biochemical analysis.

Purification of Wax from Plant Cuticle

Following excision from plants, leaf surface areas were measured and logged. Leaf surfaces were washed for 30 s in 15 mL of high-performance liquid chromatography-grade hexane (Sigma). The hexane solvent and dissolved cuticular waxes were decanted into a glass vial that had been washed with acetone and dried. Leaves were washed a second time with 2 mL of hexane, which was added to the appropriate sample vial. Hexane was evaporated under a continuous stream of N_2 to dryness, and the cuticle wax was redissolved in 250 μL of hexane.

Spontaneous Raman Spectroscopy

Spontaneous Raman spectra of purified wax samples were acquired using a Renishaw RM100 Raman microscope equipped with a 785-nm diode laser and a 1,200 line mm^{-1} spectral grating, which gave a spectral resolution of 1 cm^{-1}. Samples were mounted on aluminum-coated microscope slides.

SRS Microscopy

A detailed technical explanation of the materials and methods for SRS microscopy is provided to promote the implementation of the technique as widely as possible.

For stimulated Raman gain microscopy, two laser systems were used: The Stokes beam was provided by the signal output from the picosecond Optical Parametric Oscillator (Levante, Emerald APE) pumped by the frequency doubled output from a neodymium vanadate ps oscillator (picoTrain, HighQ laser). The pump beam was provided by a titanium sapphire laser (MIRA 900 D,

Coherent) tuned to 770 nm and operating in ps mode, which was electronically synchronized to the neodymium vanadate laser (Coherent, Synchro-lock AP), thereby ensuring the laser pulses were temporally overlapped.

The 770-nm pump beam was amplitude modulated at 1.7 MHz using an acousto-optical modulator (Crystal Technology, model 3080-122) and combined with the signal output from the optical parametric oscillator using an 850-nm short-pass dichroic mirror. Imaging was performed using a modified confocal laser scanning unit (Flouview 300, Olympus) and Olympus IX71 inverted microscope. The laser light was focused onto the sample using a 60× 1.2 numerical aperture water immersion microscope objective (UPlanS Apo, Olympus). The transmitted light from the sample was collected with a 60× 1.0 numerical aperture water-dipping condenser (LUMFI, Olympus). The transmitted Stokes beam was detected using an silicon photodiode (Thorlabs, FDS1010) with a 70-V reverse bias. The pump beam was blocked from the photodiode using an 850-nm-long pass filter (hq850lp, Chroma Technologies). The output from the photodiode was passed through a long-pass filter (minicircuits, BLP-1.9+) to remove modulations at the 76-laser repetition rate and terminated by a 50-Ω resistor. The filtered beam was then fed into a lock-in amplifier (Zurich Instruments, HF2L1 Lock-in Amplifier) that separated out the modulated SRS signal at 1.7 MHz. SRS spectra were obtained by tuning wavelength of signal beam in 0.2-nm intervals and acquiring a series of images.

Stimulated Raman gain was measured in preference to stimulated Raman loss, as it allowed the chemically specific Raman signal to be separated from any additional signal due to two photon absorption (Ye et al., 2009) or photothermal lensing (Lu et al., 2010; Moger et al., 2012) by phase-sensitive lock-in detection (Mansfield et al., 2013).

Fresh, excised plant leaves were mounted in perfluorodecalin (Littlejohn et al., 2010) prior to imaging, which has been shown not to interfere with Raman-based imaging in plants (Mansfield et al., 2013; Littlejohn et al., 2014).

SEM

Leaf samples were imaged using cryogenic SEM. Samples were flash frozen in liquid N_2 slush, transferred to a vacuum, and coated in gold using the Gatan Alto 2100 system. Images were acquired using a JEOL JSM-6390 LV scanning electron microscope operating at 5 kV with a working distance of 10 to 12 nm.

Supplemental Data

Supplemental Text S1. The Raman fitting parameters for each purified cuticular wax.

ACKNOWLEDGMENTS

We thank Peter Splatt (Exeter Bioimaging Centre) for technical assistance with the SEM, James Chidlow for plant samples from the University of Exeter greenhouse collection, and Dr. Anna Amtmann (University of Glasgow) for generously providing seeds of *Thellungiella* species used.

Received January 27, 2015; accepted March 16, 2015; published March 17, 2015.

LITERATURE CITED

Aarts MG, Keijzer CJ, Stiekema WJ, Pereira A (1995) Molecular characterization of the *CER1* gene of Arabidopsis involved in epicuticular wax biosynthesis and pollen fertility. Plant Cell **7:** 2115–2127

Amtmann A (2009) Learning from evolution: *Thellungiella* generates new knowledge on essential and critical components of abiotic stress tolerance in plants. Mol Plant **2:** 3–12

Baker EA, Holloway PJ (1971) Scanning electron microscopy of waxes on plant surfaces. Micron **2:** 364–380

Barthlott W, Neinhuis C (1997) Purity of the sacred lotus, or escape from contamination in biological surfaces. Planta **202:** 1–8

Barthlott W, Neinhuis C, Cutler D, Ditsch F, Meusel I, Theisen I, Wilhelmi H (2008) Classification and terminology of plant epicuticular waxes. Bot J Linn Soc **126:** 237–260

Beisson F, Li-Beisson Y, Pollard M (2012) Solving the puzzles of cutin and suberin polymer biosynthesis. Curr Opin Plant Biol **15:** 329–337

Bernard A, Domergue F, Pascal S, Jetter R, Renne C, Faure JD, Haslam RP, Napier JA, Lessire R, Joubès J (2012) Reconstitution of plant alkane biosynthesis in yeast demonstrates that *Arabidopsis* ECERIFERUM1 and ECERIFERUM3 are core components of a very-long-chain alkane synthesis complex. Plant Cell **24:** 3106–3118

Bessire M, Chassot C, Jacquat AC, Humphry M, Borel S, Petétot JMC, Métraux JP, Nawrath C (2007) A permeable cuticle in Arabidopsis leads to a strong resistance to *Botrytis cinerea*. EMBO J **26:** 2158–2168

Bhushan B, Jung YC (2006) Micro- and nanoscale characterization of hydrophobic and hydrophilic leaf surfaces. Nanotechnology **17:** 2758–2772

Bhushan B, Jung YC, Koch K (2009) Micro-, nano- and hierarchical structures for superhydrophobicity, self-cleaning and low adhesion. Philos Trans A Math Phys Eng Sci **367:** 1631–1672

Bourdenx B, Bernard A, Domergue F, Pascal S, Léger A, Roby D, Pervent M, Vile D, Haslam RP, Napier JA, et al (2011) Overexpression of Arabidopsis *ECERIFERUM1* promotes wax very-long-chain alkane biosynthesis and influences plant response to biotic and abiotic stresses. Plant Physiol **156:** 29–45

Buschhaus C, Hager D, Jetter R (2014) Wax layers on *Cosmos bipinnatus* petals contribute unequally to the total petal water resistance. Plant Physiol **167:** 80–88

Delventhal R, Falter C, Strugala R, Zellerhoff N, Schaffrath U (2014) Ectoparasitic growth of *Magnaporthe* on barley triggers expression of the putative barley wax biosynthesis gene CYP96B22, which is involved in penetration resistance. BMC Plant Biol **14:** 26

Ding SY, Liu YS, Zeng Y, Himmel ME, Baker JO, Bayer EA (2012) How does plant cell wall nanoscale architecture correlate with enzymatic digestibility? Science **338:** 1055–1060

Freudiger CW, Min W, Saar BG, Lu S, Holtom GR, He C, Tsai JC, Kang JX, Xie XS (2008) Label-free biomedical imaging with high sensitivity by stimulated Raman scattering microscopy. Science **322:** 1857–1861

Gilbert RD, Johnson AM, Dean RA (1996) Chemical signals responsible for appressorium formation in the rice blast fungus *Magnaporthe grisea*. Physiol Mol Plant Pathol **48:** 335–346

Greene PR, Bain CD (2005) Total internal reflection Raman spectroscopy of barley leaf epicuticular waxes in vivo. Colloids Surf B Biointerfaces **45:** 174–180

Gierlinger N, Keplinger T, Harrington M (2012) Imaging of plant cell walls by confocal Raman microscopy. Nat Protoc **7:** 1694–1708

Gierlinger N, Luss S, König C, Konnerth J, Eder M, Fratzl P (2010) Cellulose microfibril orientation of *Picea abies* and its variability at the micron-level determined by Raman imaging. J Exp Bot **61:** 587–595

Grncarevic M, Radler F (1967) The effect of wax components on cuticular transpiration-model experiments. Planta **75:** 23–27

Heredia-Guerrero JA, Benítez JJ, Domínguez E, Bayer IS, Cingolani R, Athanassiou A, Heredia A (2014) Infrared and Raman spectroscopic features of plant cuticles: a review. Front Plant Sci **5:** 305

Hen-Avivi S, Lashbrooke J, Costa F, Aharoni A (2014) Scratching the surface: genetic regulation of cuticle assembly in fleshy fruit. J Exp Bot **65:** 4653–4664

Ho M, Pemberton JE (1998) Alkyl chain conformation of octadecylsilane stationary phases by Raman spectroscopy. 1. Temperature dependence. Anal Chem **70:** 4915–4920

Jetter R, Schäffer S, Riederer M (2000) Leaf cuticular waxes are arranged in chemically and mechanically distinct layers: evidence from *Prunus laurocerasus* L. Plant Cell Environ **23:** 619–628

Jun JH, Song Z, Liu Z, Nikolau BJ, Yeung ES, Lee YJ (2010) High-spatial and high-mass resolution imaging of surface metabolites of Arabidopsis thaliana by laser desorption-ionization mass spectrometry using colloidal silver. Anal Chem **82:** 3255–3265

Kim KW, Lee ST, Bae SW, Kim PG (2011) 3D surface profiling and high resolution imaging for refining the florin rings and epicuticular wax crystals of *Pinus koraiensis* needles. Microsc Res Tech **74:** 1166–1173

Koch K, Bhushan B, Barthlott W (2009) Multifunctional surface structures of plants: an inspiration for biomimetics. Prog Mater Sci **54:** 137–178

Koch K, Neinhuis C, Ensikat HJ, Barthlott W (2004) Self assembly of epicuticular waxes on living plant surfaces imaged by atomic force microscopy (AFM). J Exp Bot **55:** 711–718

Kolattukudy PE (1981) Structure, biosynthesis, and biodegradation of cutin and suberin. Annu Rev Plant Physiol **32:** 539–567

Koornneef M, Hanhart CJ, Thiel F (1989) A genetic and phenotypic description of *eceriferum* (*cer*) mutants in *Arabidopsis thaliana*. J Hered **80:** 118–122

Krauss P, Markstadter C, Riederer M (1997) Attenuation of UV radiation by plant cuticles from woody species. Plant Cell Environ **20:** 1079–1085

Lee YH, Dean RA (1994) Hydrophobicity of contact surface induces appressorium formation in *Magnaporthe grisea*. FEMS Microbiol Lett **115:** 71–75

Littlejohn GR, Gouveia JD, Edner C, Smirnoff N, Love J (2010) Perfluorodecalin enhances in vivo confocal microscopy resolution of *Arabidopsis thaliana* mesophyll. New Phytol **186:** 1018–1025

Littlejohn GR, Mansfield JC, Christmas JT, Witterick E, Fricker MD, Grant MR, Smirnoff N, Everson RM, Moger J, Love J (April 23, 2014) An update: improvements in imaging perfluorocarbon-mounted plant leaves with implications for studies of plant pathology, physiology, development and cell biology. Front Plant Sci http://dx.doi.org/10.3389/fpls.2014.00140

Lu S, Min W, Chong S, Holtom GR, Xie XS (2010) Label-free imaging of heme proteins with two-photon excited photothermal lens microscopy. Appl Phys Lett **96:** 113701

Ly S, McNerney G, Fore S, Chan J, Huser T (2007) Time-gated single photon counting enables separation of CARS microscopy data from multiphoton-excited tissue autofluorescence. Opt Express **15:** 16839–16851

Mansfield JC, Littlejohn GR, Seymour MP, Lind RJ, Perfect S, Moger J (2013) Label-free chemically specific imaging in planta with stimulated Raman scattering microscopy. Anal Chem **85:** 5055–5063

Min W, Freudiger CW, Lu SJ, Xie XS (2011) Coherent nonlinear optical imaging: beyond fluorescence microscopy. Annu Rev Phys Chem **62:** 507–530

Moger J, Garrett NL, Begley D, Mihoreanu L, Lalatsa A, Lozano MV, Mazza M, Schatzlein A, Uchegbu I (2012) Imaging cortical vasculature with stimulated Raman scattering and two-photon photothermal lensing microscopy. J Raman Spectrosc **43:** 668–674

Pighin JA, Zheng H, Balakshin LJ, Goodman IP, Western TL, Jetter R, Kunst L, Samuels AL (2004) Plant cuticular lipid export requires an ABC transporter. Science **306:** 702–704

Raffaele S, Leger A, Roby D (2009) Very long chain fatty acid and lipid signaling in the response of plants to pathogens. Plant Signal Behav **4:** 94–99

Ristic Z, Jenks MA (2002) Leaf cuticle and water loss in maize lines differing in dehydration avoidance. J Plant Physiol **159:** 645–651

Samuels L, Kunst L, Jetter R (2008) Sealing plant surfaces: cuticular wax formation by epidermal cells. Annu Rev Plant Biol **59:** 683–707

Snyder R, Hsu S, Krimm S (1978) Vibrational spectra in the C—H stretching region and the structure of the polymethylene chain. Spectrochim Acta [A] **34:** 395–406

Teusink RS, Rahman M, Bressan RA, Jenks MA (2002) Cuticular waxes on Arabidopsis thaliana close relatives Thellungiella halophila and Thellungiella parvula. Int J Plant Sci **163:** 309–315

Veraverbeke EA, Van Bruaene N, Van Oostveldt P, Nicolaï BM (2001) Non destructive analysis of the wax layer of apple (*Malus domestica* Borkh.) by means of confocal laser scanning microscopy. Planta **213:** 525–533

Weissflog I, Vogler N, Akimov D, Dellith A, Schachtschabel D, Svatos A, Boland W, Dietzek B, Popp J (2010) Toward in vivo chemical imaging of epicuticular waxes. Plant Physiol **154:** 604–610

Xu X, Feng J, Lü S, Lohrey GT, An H, Zhou Y, Jenks MA (2014) Leaf cuticular lipids on the Shandong and Yukon ecotypes of saltwater cress, *Eutrema salsugineum*, and their response to water deficiency and impact on cuticle permeability. Physiol Plant **151:** 446–458

Ye T, Fu D, Warren WS (2009) Nonlinear absorption microscopy. Photochem Photobiol **85:** 631–645

Yeats TH, Rose JKC (2013) The formation and function of plant cuticles. Plant Physiol **163:** 5–20

Yu MML, Konorov SO, Schulze HG, Blades MW, Turner RFB, Jetter R (2008) In situ analysis by microspectroscopy reveals triterpenoid compositional patterns within leaf cuticles of *Prunus laurocerasus*. Planta **227:** 823–834

Yu Y, Ramachandran PV, Wang MC (2014) Shedding new light on lipid functions with CARS and SRS microscopy. Biochim Biophys Acta **1841:** 1120–1129

Zeng Y, Saar B, Friedrich M, Chen F, Liu YS, Dixon R, Himmel M, Xie X, Ding SY (2010) Imaging lignin-downregulated alfalfa using coherent anti-Stokes Raman scattering microscopy. BioEnergy Research **3:** 272–277

Zumbusch A, Holtom GR, Xie XS (1999) Three-dimensional vibrational imaging by coherent anti-Stokes Raman scattering. Phys Rev Lett **82:** 4142–4145